Sakarya University Journal of Computer and Information Sciences
http://saucis.sakarya.edu.tr/

DOI: 10.35377/saucis...1356872 RESEARCH ARTICLE

Estimation of Uplink Channels for Multiple Users Using Tensor Modeling in RIS-Aided MISO Communication

Rıfat Volkan Şenyuva [1]

[1]Maltepe University, Faculty of Engineering and Natural Sciences, Department of Electrical and Electronics Engineering; İstanbul, Türkiye

Corresponding author:
Rıfat Volkan Şenyuva
Maltepe University, Faculty of Engineering and Natural Sciences, Department of Electrical and Electronics Engineering; İstanbul, Türkiye
E-mail address:
rifatvolkansenyuva@maltepe.edu.tr

Submitted: 07 September 2023
Revision Requested: 05 November 2023
Last Revision Received: 07 November 2023
Accepted: 09 November 2023
Published Online: 30 November 2023

Citation: Şenyuva R.V. (2023). Estimation of Uplink Channels for Multiple Users Using Tensor Modeling in RIS-Aided MISO Communication. *Sakarya University Journal of Computer and Information Sciences.* 6 (3) https://doi.org/10.35377/saucis...1356872

ABSTRACT

In this paper estimation of uplink channels using tensor modeling is addressed for multiple users in a reconfigurable intelligent surface (RIS)-aided multiple-input single-output (MISO) communication. The coherence interval is divided into structured frames of pilot symbols transmitted by the users and pattern of phase shifts applied by the RIS in order to estimate the base station (BS)-RIS channels and the RIS-user's channels. Estimation methods that use tensor modeling including Khatri-Rao Factorization (KRF) and bilinear alternating least squares (BALS) are applied to the signal model. Numerical results show that both KRF and BALS are superior to the LS estimator by 10 dB SNR for the correlated Rayleigh fading channel model.

Keywords: Reconfigurable Intelligent Surfaces, Multi-User MISO, Channel Estimation, Least Squares, Khatri-Rao Factorization, Parallel Factor Decomposition

1. Introduction

Energy consumption is an important concern for the emerging wireless networks such as 5G [1-2], 6G [2], the Internet of Things (IoT) [2], geostationary (GEO) satellite communications (SatCom) [3-4]. A massive number of devices such as mobile phones, sensors [2], and smart sockets [5] that require uninterrupted connectivity and increased quality of service (QoS) [6] are expected to be deployed in IoT. Thus, these wireless networks must be energy efficient to be realized [1]. One of the solutions is providing some control over the propagation environment via the concept of a smart radio environment [2].

A reconfigurable intelligent surface (RIS) is a candidate technology for making these emerging networks energy efficient. The RIS comprises many low-cost antennas or metamaterials on a 2D surface with integrated circuits that can passively shape an incoming electromagnetic field in desired ways [1-2]. The phase shift of each element of the RIS can be tuned so that the reflected signals can be coherently combined such that the whole incoming signal is amplified. The energy consumption of the RIS is much less compared to that of an Amplify-and-Forward (AF) relay transceiver since the RIS does not employ power amplifiers [7]. The RIS hardware can be easily deployed in a communication environment since they do not take up much space.

One of the fundamental challenges in RIS-employed systems is obtaining the state information of the base station (BS)-RIS channel and the RIS-user channel. However, RIS with many elements means the system will have many channel links that must be estimated. In addition to this, the channels must be estimated at the receiver since no signal processing can be done

at the RIS due to the passive elements. The channel estimation problem is tackled by several previous works in the literature [8-16]. [8] shows the optimal selection for the activation pattern of the RIS elements using a minimum variance unbiased (MVU) estimator. [9] proposes a minimum mean squared error (MMSE) estimator for a deterministically scattered BS-RIS channel. A comparison of the MVU and the MMSE estimators is shown for a single user in [10]. A three-phase channel estimation protocol is given in [11] to deal with the BS-user channel or the direct channel by using the first phase to estimate the direct channel and then applying interference cancellation in the second phase. [12] applies the Khatri-Rao factorization (KRF) and bilinear alternating least squares (BALS) methods to estimate the downlink channels for a single user with multiple antennas. Channel estimation for multiple users using BALS is investigated in [13-15]. The tensor-based channel estimation in a system with double RIS is studied by [16].

We investigate the uplink channel estimation for multiple users in a RIS-aided multiple-input single-output (MISO) communication operating in a time division duplex (TDD). Compared to the conference paper [10], where there is only one user, we consider channel estimation for multiple users in this work. We focus on applying the tensor-based channel estimation methods, which decouple the estimation of the BS-RIS and the RIS-user's channels with the direct channel between the BS and users considered unavailable, unlike the signal model in [10]. Our signal model employs the pilot symbols and the RIS phase shift structure of [9,12]. We apply the two tensor-based channel estimation methods, KRF and BALS, to our multiple-user signal model. Our KRF implementation differs from that of [12] since it's built upon the least squares (LS) filtered signal and does not require the bilinear filtering step given in [12]. The performances of the algorithms are numerically evaluated for a multiple-user scenario with the channels modeled more realistically according to correlated Rayleigh fading, unlike the results given in [12-15] for uncorrelated Rayleigh fading.

The contributions of the paper can be summarized as follows:

- To the best of our knowledge, our formulation for the KRF method is the first in the literature that uses the output of the LS estimator as its input rather than the bilinear filtered signal given in [12].
- The proposed KRF method with the LS estimator is computationally efficient compared to the KRF method using bilinear filtering [12] since the LS estimator can be applied as a Fast Fourier Transform (FFT).
- We use the more practical correlated Rayleigh fading as our channel model. Our numerical results differ from the rest of the literature [12-15] in showing the impact of spatial correlation of the channels concerning RIS elements on the performance of the channel estimation methods using tensor modeling.

The remaining parts of this paper are organized in the following way: the discrete-time baseband received signal model of the MISO system is introduced in Section 2. Then, the derivations of the channel estimation methods, including the LS, KRF, and BALS, are given in Section 3. The performances of the investigated methods are compared in Section 4. Finally, Section 6 presents the conclusions of the paper.

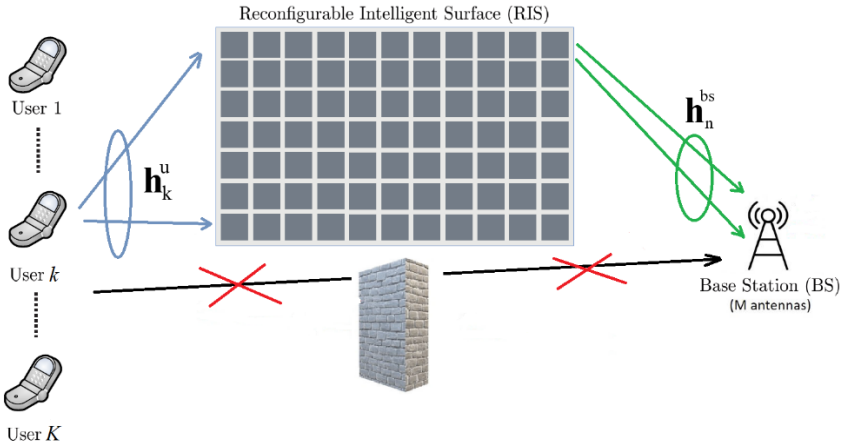

Figure 1 ***K*** single antenna users being communicating with an ***M*** -antenna BS in a RIS-assisted multi-user MISO system. Blue and green lines show the uplink channel vectors that must be estimated. The BS-users channel or the direct channel (black line with red cross) is ignored because of high attenuation.

2. System Model

We consider a narrow band MISO communication system with a BS equipped with M antennas serving K single-antenna users simultaneously, as seen in Figure 1. A RIS with N passive reflecting elements, which can only shift the phases of the impinging waves, is deployed to assist the BS. The RIS is attached to a surrounding building's façade, and the phase shift of

each RIS element can be adjusted by the BS over a backhaul link. The direct channels between the BS and any K users are ignored due to high attenuation or can be estimated by turning off the RIS elements.

The MISO system shown in Figure 1 operates in half-duplex TDD mode where the channel between antennas is the same in both directions within the coherence interval. Once the BS learns the uplink channel from uplink pilots sent by the users in the training step, it also automatically has an estimate of the downlink channel. So, a quasi-static block fading channel model, where the channels are constant within the coherence interval of T_C time slots, is assumed. The total channel training time T_C is divided into S sub-blocks where each sub-block has T time slots so that $T_C = ST$. While the RIS phase shifts are kept fixed for the duration the s-th sub-block that is T time slots, the users transmit the same pilot sequence across the S sub-blocks [9,12]. The received baseband signal at the t-th time slot of the s-th sub-block $\mathbf{y}_{s,t} \in \mathbb{C}^{M\times 1}$, is given as

$$\mathbf{y}_{s,t} = \mathbf{H}^{\text{bs}}(\boldsymbol{\phi}_s \odot \mathbf{H}^{\text{u}}\mathbf{x}_t) + \mathbf{n}_{s,t} \tag{1}$$

where the channels between the RIS and BS are shown as $\mathbf{H}^{\text{bs}} = \left[\mathbf{h}_1^{\text{bs}} \dots \mathbf{h}_N^{\text{bs}}\right] \in \mathbb{C}^{M\times N}$, the channels between the users and the RIS are represented as $\mathbf{H}^{\text{u}} = [\mathbf{h}_1^{\text{u}} \dots \mathbf{h}_K^{\text{u}}] \in \mathbb{C}^{N\times K}$, $\mathbf{x}_t \in \mathbb{C}^{K\times 1}$ show the orthogonal pilot sequence transmitted by the users, and $\mathbf{n}_{s,t} \in \mathbb{C}^{M\times 1}$ shows the complex additive white Gaussian noise random vector with single-sided power spectral density of N_0, i.e. $\mathbf{n}_{s,t} \sim \mathcal{CN}(\mathbf{0}, N_0\mathbf{I}_M)$ where $\mathbf{I}_M$ is the $M \times M$ identity matrix. The RIS phase shift vector applied at the s-th sub-block is given as $\boldsymbol{\phi}_s = [e^{i\theta_{1,s}}, \dots, e^{i\theta_{N,s}}]^{\text{T}} \in \mathbb{C}^{N\times 1}$ where $\theta_{n,s} \in (\mathbf{0}, 2\pi]$, and $\odot$ is the element-wise multiplication, i.e. the Hadamard product shown as with $\mathbf{H}^{\text{u}}\mathbf{x}_t$ in Equation 1. $\mathbf{h}_n^{\text{bs}}$ and $\mathbf{h}_k^{\text{u}}$ are modeled as correlated Rayleigh channels.

$$\mathbf{h}_n^{\text{bs}} = \sqrt{\beta_n^{\text{bs}}}\mathbf{K}_n^{1/2}\mathbf{g}_n \tag{2}$$

$$\mathbf{h}_k^{\text{u}} = \sqrt{\beta_k^{u}}\mathbf{K}_k^{1/2}\mathbf{g}_k \tag{3}$$

where $\mathbf{K}_n^{1/2}$ and $\mathbf{K}_k^{1/2}$ are the correlation matrices at the BS and IRS respectively. $\mathbf{g}_n \sim \mathcal{CN}(\mathbf{0}, \mathbf{I}_M)$ and $\mathbf{g}_k \sim \mathcal{CN}(\mathbf{0}, \mathbf{I}_N)$ are the fast-fading components while $\boldsymbol{\beta}_n^{\text{bs}}$ and $\boldsymbol{\beta}_k^{\text{u}}$ are the path loss factors. The received signals for the s-th sub-block, $\mathbf{Y}_s = [\mathbf{y}_{s,1}, \dots, \mathbf{y}_{s,T}] \in \mathbb{C}^{M\times T}$, can be written as

$$\mathbf{Y}_s = \mathbf{H}^{\text{bs}}\text{diag}\{\boldsymbol{\phi}_s\}\mathbf{H}^{\text{u}}\mathbf{X} + \mathbf{N}_s \tag{4}$$

where $\text{diag}\{\boldsymbol{\phi}_s\}$ is the matrix with the elements of $\boldsymbol{\phi}_s$ on its diagonal, $\mathbf{X} = [\mathbf{x}_1, \dots, \mathbf{x}_T] \in \mathbb{C}^{K\times T}$ is the pilot sequence matrix across the T slots, and the noise matrix for the s-th sub-block is denoted as $\mathbf{N}_s = [\mathbf{n}_{s,1}, \dots, \mathbf{n}_{s,T}] \in \mathbb{C}^{M\times T}$. The receiver first despreads the received signal in Equation 4 by multiplying with Hermitian transpose of $\mathbf{X}$, i.e., $\mathbf{X}^{\text{H}}$, resulting in

$$\widetilde{\mathbf{Y}}_s = \mathbf{H}^{\text{bs}}\text{diag}\{\boldsymbol{\phi}_s\}\mathbf{H}^{\text{u}} + \widetilde{\mathbf{N}}_s \tag{5}$$

where $\widetilde{\mathbf{Y}}_s = \mathbf{Y}_s\mathbf{X}^{\text{H}}$, $\widetilde{\mathbf{N}}_s = \mathbf{N}_s\mathbf{X}^{\text{H}}$, and the size of both matrices is $M \times K$. Due to the pilot sequence matrix, $\mathbf{X}$, being a unitary matrix, i.e., $\mathbf{X}\mathbf{X}^{\text{H}} = \mathbf{I}$, the distribution of the noise vectors in $\widetilde{\mathbf{N}}_s$ do not change.

3. Channel Estimation Methods

Channel estimation schemes take the received signal $\widetilde{\mathbf{Y}}_s$ in Equation 5 as input and output an estimate of either each of the channel matrices $\mathbf{H}^{\text{bs}}$ and $\mathbf{H}^{\text{u}}$ or the cascade channel matrix which is the product of the individual channel matrices. The least squares method estimates the cascade channel matrix while the KRF and the BALS method estimate $\mathbf{H}^{\text{bs}}$ and $\mathbf{H}^{\text{u}}$ separately. Estimating the channel matrices separately is subject to complex scaling ambiguity, but the scaling factors cancel each other when the separate channel matrices are multiplied to calculate the cascade channel.

3.1 Least Squares Channel Estimation

Least squares (LS) estimation is a benchmark method of estimating the cascade channel matrix. If both sides of the Equation 5 are vectorized, since $\text{diag}\{\boldsymbol{\phi}_s\}$ is a diagonal matrix, it can be rewritten by using the properties $\text{vec}\{\mathbf{ABC}\} = (\mathbf{C}^{\text{T}} \diamond \mathbf{A})\text{vecd}\{\mathbf{B}\}$ as

$$\mathbf{r}_s = (\bar{\mathbf{H}}^{\text{u}} \diamond \mathbf{H}^{\text{bs}})\boldsymbol{\phi}_s + \mathbf{w}_s \tag{6}$$

where $\mathbf{r}_s = \text{vec}\{\widetilde{\mathbf{Y}}_s\} \in \mathbb{C}^{MK\times 1}$, $\mathbf{w}_s = \text{vec}\{\widetilde{\mathbf{N}}_s\} \in \mathbb{C}^{MK\times 1}$, $\bar{\mathbf{H}}^{\text{u}} = [\mathbf{H}^{\text{u}}]^{\text{T}} \in \mathbb{C}^{K\times N}$ that is the transpose of $\mathbf{H}^{\text{u}}$, $\diamond$ denotes the Khatri-Rao product. If $\mathbf{R} = [\mathbf{r}_1 \dots \mathbf{r}_S] \in \mathbb{C}^{MK\times S}$ and $\mathbf{W} = [\mathbf{w}_1 \dots \mathbf{w}_S] \in \mathbb{C}^{MK\times S}$ are defined, then $\mathbf{R}$ is equal to

$$\mathbf{R} = \mathbf{H}^{\text{cascade}}\boldsymbol{\Phi} + \mathbf{W} \tag{7}$$

where $\mathbf{H}^{\text{cascade}} = \left[\bar{\mathbf{H}}^{\text{u}} \diamond \mathbf{H}^{\text{bs}}\right] \in \mathbb{C}^{MK\times N}$ and $\boldsymbol{\Phi} = [\boldsymbol{\phi}_1 \dots \boldsymbol{\phi}_S] \in \mathbb{C}^{N\times S}$. Applying another vectorization to both sides of Equation 7 and then using the property $\text{vec}\{\mathbf{ABC}\} = (\mathbf{C}^{\text{T}} \otimes \mathbf{A})\text{vec}\{\mathbf{B}\}$ yields

$$\mathbf{r}' = (\bar{\mathbf{\Phi}} \otimes \mathbf{I}_{MK})\text{vec}\{\mathbf{H}^{\text{cascade}}\} + \mathbf{z} \tag{8}$$

where $\mathbf{r}' = \text{vec}\{\mathbf{R}\} \in \mathbb{C}^{MKS\times 1}$, $\mathbf{z} = \text{vec}\{\mathbf{W}\} \in \mathbb{C}^{MKS\times 1}$, $\bar{\mathbf{\Phi}} = \mathbf{\Phi}^{\text{T}} \in \mathbb{C}^{S\times N}$ that is the transpose of $\mathbf{\Phi}$ and $\otimes$ denotes the Kronecker product. Equation 8 can be rewritten as

$$\mathbf{r}' = \mathbf{Q}\mathbf{h}^{\text{cascade}} + \mathbf{z} \tag{9}$$

where $\mathbf{Q} = [\bar{\mathbf{\Phi}} \otimes \mathbf{I}_{MK}] \in \mathbb{C}^{MKS\times MKN}$ and $\mathbf{h}^{\text{cascade}} = \text{vec}\{\mathbf{H}^{\text{cascade}}\} \in \mathbb{C}^{MKN\times 1}$. The LS estimate is obtained from

$$\hat{\mathbf{h}}^{\text{cascade}} = \underset{\mathbf{h}^{\text{cascade}}}{\arg\min} \left\|\mathbf{r}' - \mathbf{Q}\mathbf{h}^{\text{cascade}}\right\|_2^2 \tag{10}$$

where the solution is equal to $\hat{\mathbf{h}}^{\text{cascade}} = \mathbf{Q}^{\dagger}\mathbf{r}'$ provided that $S \geq N$ holds and $\mathbf{Q}^{\dagger}$ is the Moore-Penrose left inverse of $\mathbf{Q}$. The LS estimate can be simplified to

$$\hat{\mathbf{h}}^{\text{cascade}} = [(\bar{\mathbf{\Phi}}^{\text{H}}\bar{\mathbf{\Phi}})^{-1}\bar{\mathbf{\Phi}}^{\text{H}} \otimes \mathbf{I}_{MK}]\mathbf{r}' \tag{11}$$

where $\bar{\mathbf{\Phi}}^{\text{H}}$ is the conjugate transpose of $\bar{\mathbf{\Phi}}$. [8-9] shows that constructing $\bar{\mathbf{\Phi}}$ from the S leading columns of the $N \times N$ DFT matrix, $\mathbf{F} \in \mathbb{C}^{N\times S}$, as

$$[\bar{\mathbf{\Phi}}]_{s,n} = [\mathbf{F}]_{s,n} = \exp\left[-i\frac{2\pi(s-1)(n-1)}{S}\right], \qquad s = 1, \dots S, n = 1, \dots, N \tag{12}$$

minimizes the LS error. Plugging Equation 12 into Equation 11 simplifies the LS estimator expression further as

$$\hat{\mathbf{h}}^{\text{cascade}} = (1/S)[\mathbf{F}^{\text{H}} \otimes \mathbf{I}_{MK}]\mathbf{r}' \tag{13}$$

where $\mathbf{F}^{\text{H}}$ is the conjugate transpose of $\mathbf{F}$. The LS estimator in Equation 13 can be calculated is in total $\mathcal{O}(MKS\log S)$ operations due to the application of MK inverse DFT which can be implemented as FFT in $\mathcal{O}(S\log S)$ operations [8].

3.2 Khatri-Rao Factorization Based Channel Estimation

Once the LS estimator in Equation 13 is applied, we obtain

$$\tilde{\mathbf{r}} = \mathbf{h}^{\text{cascade}} + \tilde{\mathbf{z}} \tag{14}$$

where $\tilde{\mathbf{r}} = (1/\text{N})[\mathbf{F}^{\text{H}} \otimes \mathbf{I}_{MK}]\mathbf{r}'$, and $\tilde{\mathbf{z}} = (1/\text{N})[\mathbf{F}^{\text{H}} \otimes \mathbf{I}_{MK}]\mathbf{z}$. If the filtered signal, $\tilde{\mathbf{r}}$, in Equation 14 is reshaped into a $MK \times N$ matrix, then it can be written using as

$$\tilde{\mathbf{R}} = \bar{\mathbf{H}}^{\text{u}} \diamond \mathbf{H}^{\text{bs}} + \tilde{\mathbf{Z}} \tag{15}$$

where $\tilde{\mathbf{R}} = [\tilde{\mathbf{r}}_1 \dots \tilde{\mathbf{r}}_N] \in \mathbb{C}^{MK\times N}$ and $\tilde{\mathbf{Z}} = [\tilde{\mathbf{z}}_1 \dots \tilde{\mathbf{z}}_N] \in \mathbb{C}^{MK\times N}$. The Khatri-Rao least squares problem

$$\underset{\bar{\mathbf{H}}^{\text{u}},\mathbf{H}^{\text{bs}}}{\min} \left\|\tilde{\mathbf{R}} - \bar{\mathbf{H}}^{\text{u}} \diamond \mathbf{H}^{\text{bs}}\right\|_F^2 \tag{16}$$

deals with the solving both $\bar{\mathbf{H}}^{\text{u}}$ and $\mathbf{H}^{\text{bs}}$ in Equation 15 [12]. An efficient solution of the Khatri-Rao least squares problem in Equation 16 is the KRF algorithm which is shown in Algorithm 1. The n-th column of the Khatri-Rao product $\tilde{\mathbf{R}} \approx \bar{\mathbf{H}}^{\text{u}} \diamond \mathbf{H}^{\text{bs}}$ is defined as $\tilde{\mathbf{r}}_n \approx \bar{\mathbf{h}}_n^{\text{u}} \otimes \mathbf{h}_n^{\text{bs}}$ which is a collection of all pair-wise product of its elements. This collection of products can be reshaped into a rank-one matrix, $\text{vec}\{\tilde{\mathbf{R}}_n\} = \tilde{\mathbf{r}}_n$, that is the outer product of two vectors that is $\tilde{\mathbf{R}}_n = \mathbf{h}_n^{\text{bs}}(\bar{\mathbf{h}}_n^{\text{u}})^{\text{T}}$. The best rank-one approximation is known to be given by the truncated singular value decomposition (SVD). The KRF algorithm (Algorithm 1) cannot give a unique solution since there exists one non-zero complex number which results in a scaling ambiguity per column that is $\bar{\mathbf{h}}_n^{\text{u}} \otimes \mathbf{h}_n^{\text{bs}} = \left(\alpha_n\bar{\mathbf{h}}_n^{\text{u}}\right) \otimes \left(\frac{1}{\alpha_n}\mathbf{h}_n^{\text{bs}}\right) \forall \alpha_n \in \mathbb{C}_{\neq 0}$.

The computational complexity of the KRF is determined by the fourth step in Algorithm 1, which calculates the truncated SVD. N number of truncated SVD can be calculated in $\mathcal{O}(MKN)$ operations which is the complexity of the KRF algorithm [12]. The flow chart of Algorithm 1 is shown in Figure 2.

Algorithm 1 Khatri-Rao Factorization (KRF)

1	input $\tilde{\mathbf{R}}$
2	for $n = 1, \dots, N$
3	reshape n-th column of $\tilde{\mathbf{R}}$ into $\tilde{\mathbf{R}}_n \in \mathbb{C}^{M\times K}$ such that $\text{vec}\{\tilde{\mathbf{R}}_n\} = \tilde{\mathbf{r}}_n$
4	calculate the SVD of $\tilde{\mathbf{R}}_n$ as $\tilde{\mathbf{R}}_n = \mathbf{U}_n\mathbf{\Sigma}_n\mathbf{V}_n^{\text{H}}$
5	calculate the best rank-one approximations by truncating the
6	SVD as $\hat{\mathbf{h}}_n^{\text{u}} = \sqrt{\sigma_1}\mathbf{v}_1^*$ and $\hat{\mathbf{h}}_n^{\text{bs}} = \sqrt{\sigma_1}\mathbf{u}_1$ where σ_1 is the largest singular
7	value and $\mathbf{v}_1$ and $\mathbf{u}_1$ are the first columns of $\mathbf{V}_n$ and $\mathbf{U}_n$
8	end
9	output $\hat{\mathbf{H}}^{\text{u}} = [\hat{\mathbf{h}}_1^{\text{u}} \dots \hat{\mathbf{h}}_N^{\text{u}}]$ and $\hat{\mathbf{H}}^{\text{bs}} = [\hat{\mathbf{h}}_1^{\text{bs}} \dots \hat{\mathbf{h}}_N^{\text{bs}}]$

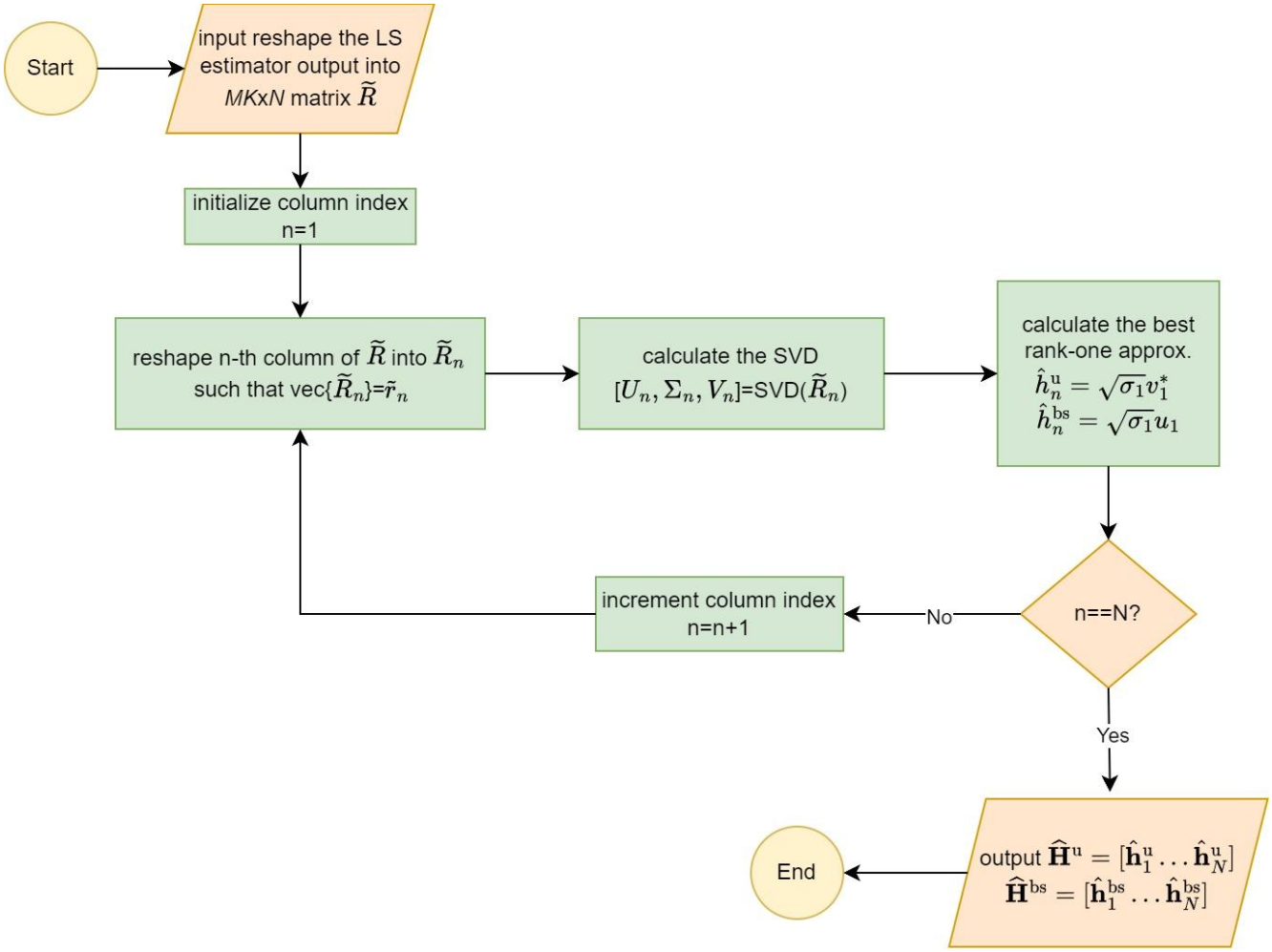

Figure 2 The flow chart of Algorithm 1.

3.3 Bilinear Alternating Least Squares Channel Estimation

The signal part of the received signal in Equation 5 is given as

$$\mathbf{Y}_s' = \mathbf{H}^{\mathrm{bs}} \mathrm{diag}\{\boldsymbol{\phi}_s\} [\bar{\mathbf{H}}^{\mathrm{u}}]^{\mathrm{T}} \tag{17}$$

where $\mathbf{Y}_s' \in \mathbb{C}^{M \times K}$. The matrix, $\mathbf{Y}_s'$, is the s-th frontal slice of a three-way signal tensor $\mathcal{Y}' \in \mathbb{C}^{M \times K \times S}$. Using the canonical parallel factor (PARAFAC) decomposition, the signal tensor $\mathcal{Y}'$ can be factorized into a sum of rank-one tensors [17-18] as

$$\mathcal{Y}' = [\![\mathbf{H}^{\mathrm{bs}}, \bar{\mathbf{H}}^{\mathrm{u}}, \bar{\boldsymbol{\Phi}}]\!] = \sum_{n=1}^{N} \mathbf{h}_n^{\mathrm{bs}} \circ \bar{\mathbf{h}}_n^{\mathrm{u}} \circ \bar{\boldsymbol{\phi}}_n \tag{18}$$

where $\circ$ denotes the outer product. $\mathcal{Y}'$ in Equation 18 can be written in three matricized forms or mode-n unfoldings [17-18] as

$$\mathbf{Y}_{(1)}' = \mathbf{H}^{\mathrm{bs}} (\bar{\boldsymbol{\Phi}} \diamond \bar{\mathbf{H}}^{\mathrm{u}})^{\mathrm{T}} \tag{19}$$

$$\mathbf{Y}_{(2)}' = \bar{\mathbf{H}}^{\mathrm{u}} (\bar{\boldsymbol{\Phi}} \diamond \mathbf{H}^{\mathrm{bs}})^{\mathrm{T}} \tag{20}$$

$$\mathbf{Y}_{(3)}' = \bar{\boldsymbol{\Phi}} (\bar{\mathbf{H}}^{\mathrm{u}} \diamond \mathbf{H}^{\mathrm{bs}})^{\mathrm{T}} \tag{21}$$

where $\mathbf{Y}_{(1)}' = [\mathbf{Y}_1', \dots, \mathbf{Y}_S'] \in \mathbb{C}^{M \times KS}$, $\mathbf{Y}_{(2)}' = [\overline{\mathbf{Y}_1'}, \dots, \overline{\mathbf{Y}_S'}] \in \mathbb{C}^{K \times MS}$, $\overline{\mathbf{Y}_s'} = [\mathbf{Y}_s']^{\mathrm{T}}$, and $\mathbf{Y}_{(3)}' = [\mathrm{vec}\{\mathbf{Y}_1'\}, \dots, \mathrm{vec}\{\mathbf{Y}_S'\}]^{\mathrm{T}} \in \mathbb{C}^{S \times MK}$. When noise is added to the signal tensor in Equation 18, the received signal tensor is given as

$$\tilde{\mathcal{Y}} = \mathcal{Y}' + \tilde{\mathcal{N}} \tag{22}$$

where the noise tensor is shown as $\tilde{\mathcal{N}}$. The mode-n unfoldings of the received signal tensor in Equation 22 are

$$\widetilde{\mathbf{Y}}_{(l)} = \mathbf{Y'}_{(l)} + \widetilde{\mathbf{N}}_{(l)} \tag{23}$$

where $l = 1,2,3$ and $\widetilde{\mathbf{N}}_{(l)}$ is the corresponding unfolding for the noise tensor, $\widetilde{\mathcal{N}}$. The bilinear alternating least squares (BALS) estimation shown in Algorithm 2 is applied to the noisy versions of Equation 19 and Equation 20 which are $\widetilde{\mathbf{Y}}_{(1)}$ and $\widetilde{\mathbf{Y}}_{(2)}$ respectively. BALS requires $\bar{\mathbf{H}}^{\mathrm{u}}$ to be initialized and this is achieved by calculating the SVD of $\mathbf{Y}'_{(2)}$ and setting $\bar{\mathbf{H}}^{\mathrm{u}}$ to N leading left singular vectors of $\mathbf{Y}'_{(2)}$. Since the RIS coefficients matrix, $\bar{\mathbf{\Phi}}$, is known and so does not need to be fixed, BALS first fixes $\bar{\mathbf{H}}^{\mathrm{u}}$ to solve for $\mathbf{H}^{\mathrm{bs}}$ by calculating

$$\hat{\mathbf{H}}^{\mathrm{bs}} = \min_{\mathbf{H}^{\mathrm{bs}}} \left\| \widetilde{\mathbf{Y}}_{(1)} - \mathbf{H}^{\mathrm{bs}} (\bar{\mathbf{\Phi}} \diamond \bar{\mathbf{H}}^{\mathrm{u}})^{\mathrm{T}} \right\|_F^2 = \widetilde{\mathbf{Y}}_{(1)} [(\bar{\mathbf{\Phi}} \diamond \bar{\mathbf{H}}^{\mathrm{u}})^{\mathrm{T}}]^{\dagger} \tag{24}$$

where $[(\bar{\mathbf{\Phi}} \diamond \bar{\mathbf{H}}^{\mathrm{u}})^{\mathrm{T}}]^{\dagger}$ is the Moore-Penrose right inverse $(\bar{\mathbf{\Phi}} \diamond \bar{\mathbf{H}}^{\mathrm{u}})^{\mathrm{T}}$ and then fixes $\mathbf{H}^{\mathrm{bs}} = \hat{\mathbf{H}}^{\mathrm{bs}}$ to solve for $\bar{\mathbf{H}}^{\mathrm{u}}$ by calculating

$$\hat{\mathbf{H}}^{\mathrm{u}} = \min_{\mathbf{H}^{\mathrm{u}}} \left\| \widetilde{\mathbf{Y}}_{(2)} - \bar{\mathbf{H}}^{\mathrm{u}} (\bar{\mathbf{\Phi}} \diamond \mathbf{H}^{\mathrm{bs}})^{\mathrm{T}} \right\|_F^2 = \widetilde{\mathbf{Y}}_{(2)} \left[(\bar{\mathbf{\Phi}} \diamond \mathbf{H}^{\mathrm{bs}})^{\mathrm{T}} \right]^{\dagger} \tag{25}$$

where $\left[(\bar{\mathbf{\Phi}} \diamond \mathbf{H}^{\mathrm{bs}})^{\mathrm{T}} \right]^{\dagger}$ is the Moore-Penrose right inverse of $(\bar{\mathbf{\Phi}} \diamond \mathbf{H}^{\mathrm{bs}})^{\mathrm{T}}$ [12-13]. The necessary condition for obtaining unique solutions to Equations 24 and 25 is that the matrices $(\bar{\mathbf{\Phi}} \diamond \bar{\mathbf{H}}^{\mathrm{u}}) \in \mathbb{C}^{SK \times N}$ and $(\bar{\mathbf{\Phi}} \diamond \mathbf{H}^{\mathrm{bs}}) \in \mathbb{C}^{SM \times N}$ must have full column rank which means $SK \geq N$ and $SM \geq N$. Satisfying these two inequalities at the same time yields $S\min(K, M) \geq N$ [12]. This condition is not sufficient to guarantee the uniqueness of the BALS estimates. For the PARAFAC decomposition in Equation 18 to be identifiable $M, K \geq N$ [13-14]. Both the number of users and the number of BS antennas of a practical MISO system is going to be less than the number of RIS elements. The identifiability condition may be satisfied by partitioning the RIS into groups of non-overlapping cells with the number of elements in each cell less than M and K [13]. The algorithm stops either when $\left\| \varepsilon_j - \varepsilon_{j-1} \right\| < \epsilon$ that is the error calculated at the j-th iteration of the algorithm, $\varepsilon_j = \left\| \tilde{\mathcal{Y}} - \hat{\mathcal{Y}}_j \right\|_F^2$, is less than a threshold, ϵ, or a maximum number of iterations, J, has been completed.

Algorithm 2 BALS

```
input Φ̄
initialize Ĥ^u by calculating SVD of Y'_(2) and set Ĥ^u to N leading
left singular vectors of Y'_(2)
for j = 1, ..., J
  find an estimate of H^bs by calculating Ĥ^bs = Y'_(1)[(Φ̄ ◇ Ĥ^u)^T]^†
  find an estimate of H̄^u by calculating Ĥ^u = Y'_(2)[(Φ̄ ◇ Ĥ^bs)^T]^†
  if ||ε_j − ε_(j−1)|| < ϵ
    break
  end
end
output Ĥ^u and Ĥ^bs
```

The computationally involved steps of the BALS estimation shown in Algorithm 2 are the fifth and sixth steps in which are the calculation of two right pseudo-inverses. The estimates of $\hat{\mathbf{H}}^{\mathrm{bs}}$ and $\hat{\mathbf{H}}^{\mathrm{u}}$ can be calculated in $\mathcal{O}(N^3 + 4N^2MS - NMS)$ and $\mathcal{O}(N^3 + 4N^2KS - NKS)$ operations [14]. Thus, the complexity of the BALS for a maximum number of iterations is equal to $\mathcal{O}(2N^3J + 4N^2SJ(M + K) - NSJ(M + K))$. The flow chart of Algorithm 2 is shown in Figure 3.

4. Numerical Results

The numerical results are calculated in a MATLAB environment of R2023b release with version number 23.2.0.2409890 and 3rd update installed on a personal computer (PC). The PC's operating system is 64-bit Windows 11 Pro with AMD Ryzen 5 3600 6-Core Processor at 3.60 GHz and 16 GB RAM. The normalized mean square error (NMSE) is used to compare the performances of the investigated estimators. NMSE can be calculated in

$$\mathrm{NMSE}(\hat{\mathbf{H}}^{o}) = \frac{1}{R} \sum_{r=1}^{R} \frac{\left\| \mathbf{H}_r - \hat{\mathbf{H}}_r^{o} \right\|_F^2}{\left\| \mathbf{H}_r \right\|_F^2} \tag{26}$$

where $o \in \{\mathrm{bs}, \mathrm{u}, \mathrm{cascade}\}$, $\hat{\mathbf{H}}_r^{o}$ is the corresponding channel matrix estimated at the r-th iteration, R is the total number of runs and $\|\cdot\|_F^2$ shows the square of the Frobenius norm. The signal-to-noise ratio (SNR) is given as

$$\mathrm{SNR} = 10\log_{10}\left(\frac{\|\mathcal{Y}'\|_F^2}{\|\widetilde{\mathcal{N}}\|_F^2}\right) \tag{27}$$

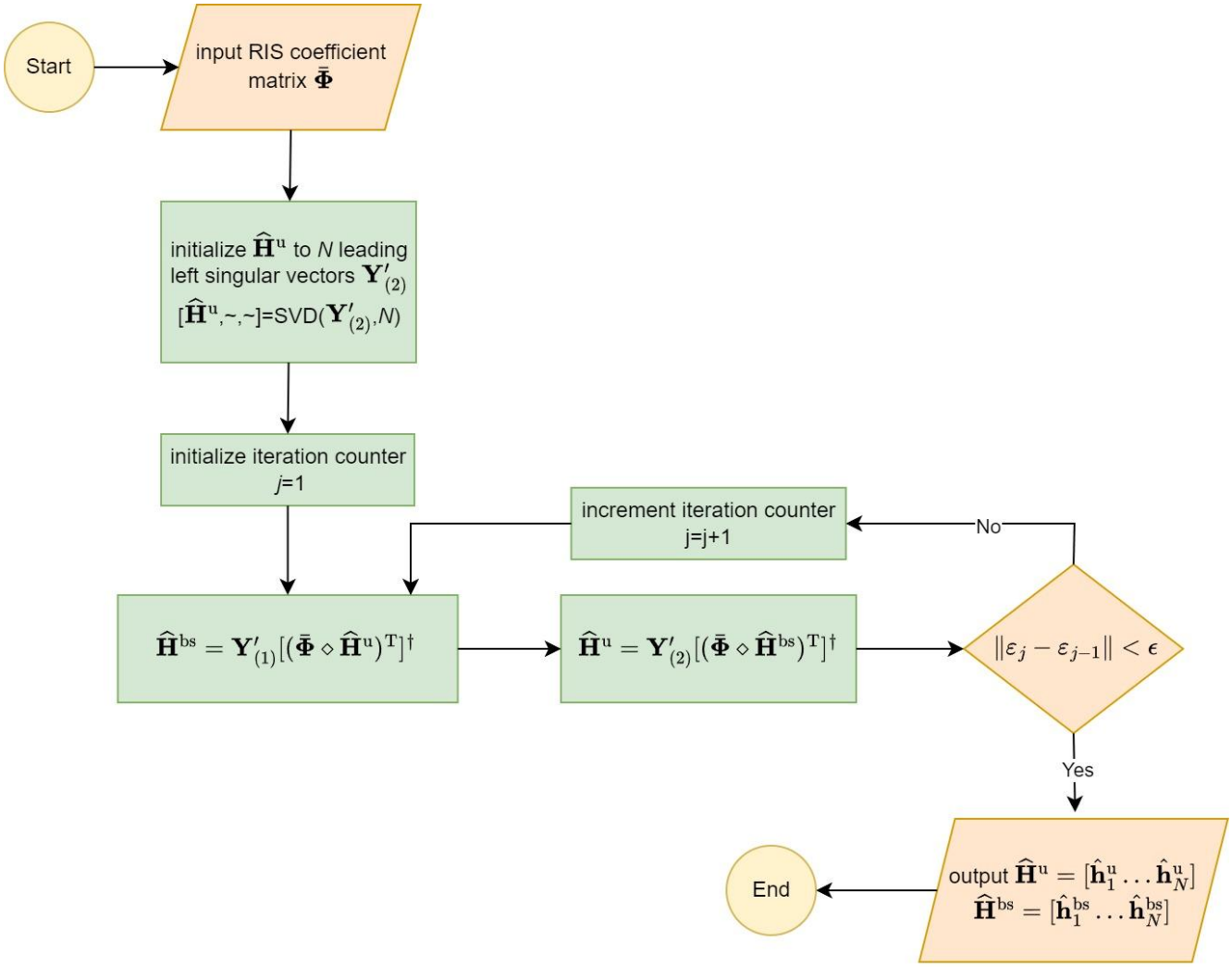

Figure 3 The flow chart of Algorithm 2.

where $\|\widetilde{\mathcal{N}}\|_F^2 = MTSN_0$. The channel matrices $\mathbf{H}^{\mathrm{bs}}$ and $\mathbf{H}^{\mathrm{u}}$ are generated as Rayleigh fading channels with correlation matrices $[\mathbf{K}_n]_{m,m'} = \eta^{|m-m'|}$ and $[\mathbf{K}_k]_{n,n'} = \eta^{|n-n'|}$ respectively with correlation coefficient set to $\eta = 0.95$ in each run. NMSE curves are averaged over $R = 1000$ iterations for parameters $M = K = T = 16$, $S = 32$, $N \in \{8,16\}$ and the SNR is within [0,30] dB. Figure 4 gives the NMSE curves for the estimation of $\mathbf{H}^{\mathrm{u}}$ and $\mathbf{H}^{\mathrm{bs}}$ separately by the KRF and BALS algorithms. The performance of the LS estimator is not available in this scenario since it can only estimate the cascade channel. The scaling ambiguity that is inherent in both the KRF and BALS algorithms separate estimation of $\mathbf{H}^{\mathrm{u}}$ and $\mathbf{H}^{\mathrm{bs}}$ is dealt with normalizing the first column of $\mathbf{H}^{\mathrm{u}}$ to an all-ones vector so that the first column $\widehat{\mathbf{H}}^{\mathrm{u}}$ gives the scaling coefficients [13-14]. We can see from Figure 4 that the performances of the KRF and the BALS algorithm are very close to each other except for $N = 16$ at 0 dB SNR where the BALS is better than the KRF in estimating $\mathbf{H}^{\mathrm{u}}$. The estimation accuracy for $\mathbf{H}^{\mathrm{bs}}$ is better than that of $\mathbf{H}^{\mathrm{u}}$ for both tensor-based approaches. Doubling of N from 8 to 16 causes approximately a 2.5 dB loss in SNR (Figure 4) due to the increased dimension of the channel coefficient vector.

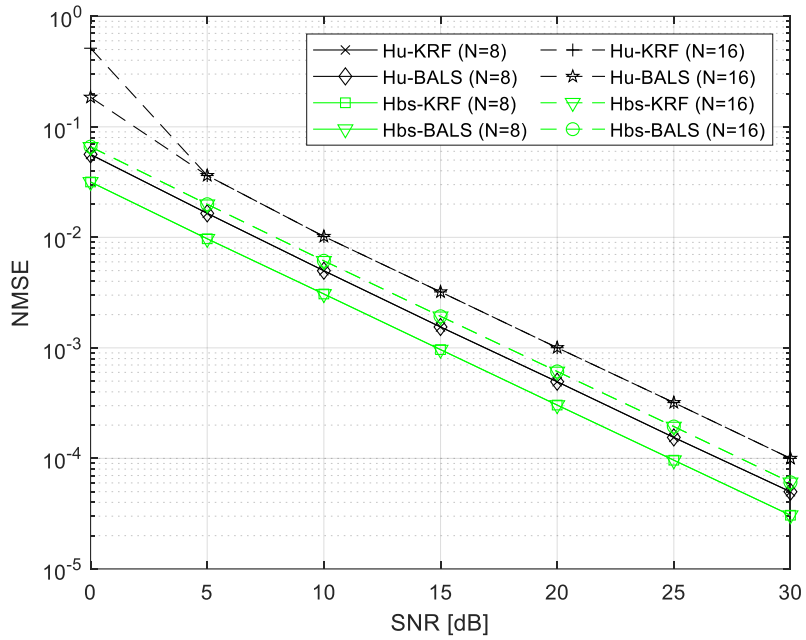

Figure 4 NMSE of $\widehat{\mathbf{H}}^{\text{bs}}$ and $\widehat{\mathbf{H}}^{\text{u}}$ for $\boldsymbol{M = K = T = 16}$, $\boldsymbol{S = 32}$, $\boldsymbol{N \in \{8, 16\}}$.

The NMSE plots for the estimation of the cascade channel, $\mathbf{H}^{\text{cascade}}$, are shown in Figure 5. The LS estimator, computationally less involved, performs the worst compared to KRF or BALS. Both tensor-based channel estimation methods improve the LS estimator by a 10 dB SNR margin. The performances of the KRF and BALS algorithms are indistinguishable regarding the cascade channel NMSE. Increasing N from 8 to 16 results in approximately 2.5 dB loss in SNR for both the LS and the tensor-based approaches.

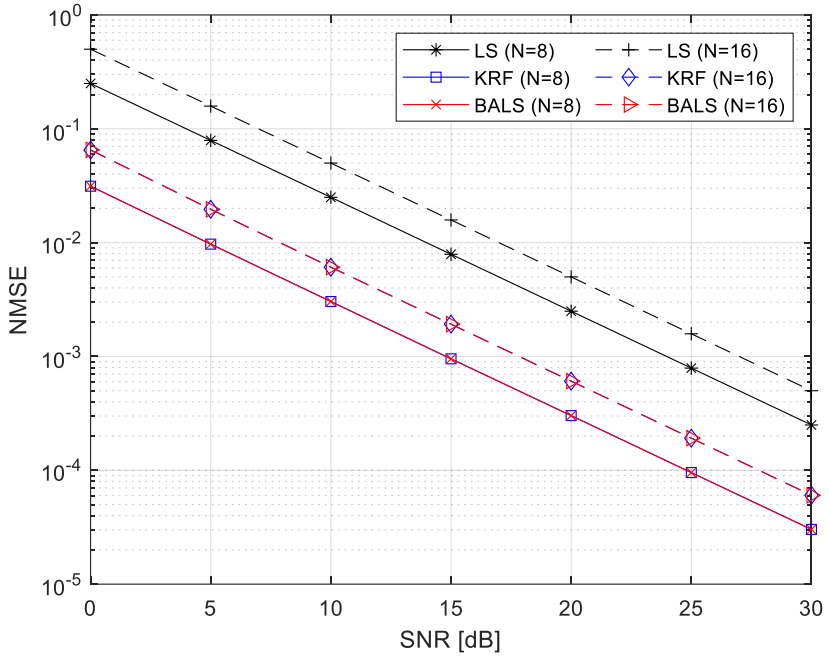

Figure 5 NMSE of $\widehat{\mathbf{H}}^{\text{cascade}}$ for $\boldsymbol{M = K = T = 16}$, $\boldsymbol{S = 32}$, $\boldsymbol{N \in \{8, 16\}}$.

5. Discussion

Since the LS estimator can be implemented using the FFT algorithm, our proposed KRF method, which takes the LS estimator as its input, has a computational advantage over the KRF method of [12], which requires a bilinear filtering step. While the

numerical results of [12] are given for only a single-user scenario, our numerical results, like those in [11,13-15], are evaluated for multiple users. We use the correlated Rayleigh fading model, which is a better model for the spatial correlation due to the RIS elements in the uplink channels. Our numerical results show its impact on the channel estimation performance unlike the rest of the literature on tensor modeling methods [12-15], which include only the results for the uncorrelated Rayleigh fading. Also, the numerical results of [13] and [15] only focus on applying the BALS algorithm and do not include the KRF method. [16] investigates the application of tensor-based channel estimation methods for double RIS-aided systems, unlike the single RIS-aided systems considered by our paper and the rest of the literature [12-15]. Compared to [14], we do not cover the achievable sum rates for the downlink communication using the channels estimated by the proposed methods in our paper. As a future work, the rate of each user can be investigated for different RIS matrix designs and precoding schemes such as maximum ratio transmission, zero forcing, and minimum mean square error schemes.

6. Conclusion

We presented applying two tensor-based channel estimation methods, KRF and BALS, to the uplink of a RIS-aided multi-user MISO communication system. The derivations, identifiability conditions, and complexities of the algorithms are given in detail. The performances of the tensor-based algorithms are numerically compared against the baseline conventional LS estimation for the correlated Rayleigh fading channel model. Numerical results show that while the performances of both tensor-based are on the same level concerning each other, both improve upon the LS estimator by a 10-dB margin. It is observed that all estimators lose 2.5 dB in SNR when the number of RIS elements is doubled.

References

[1] C. Huang, A. Zappone, G. C. Alexandropoulos, M. Debbah and C. Yuen, "Reconfigurable Intelligent Surfaces for Energy Efficiency in Wireless Communication," in *IEEE Trans. Wireless Commun.*, vol. 18, no. 8, pp. 4157-4170, Aug. 2019.

[2] M. Di Renzo *et al.*, "Smart Radio Environments Empowered by Reconfigurable Intelligent Surfaces: How It Works, State of Research, and The Road Ahead," in *IEEE J. Sel. Areas Commun.*, vol. 38, no. 11, pp. 2450-2525, Nov. 2020.

[3] W. U. Khan, E. Lagunas, A. Mahmood, B. M. ElHalawany, S. Chatzinotas and B. Ottersten, "When RIS Meets GEO Satellite Communications: A New Sustainable Optimization Framework in 6G," *IEEE VTC2022-Spring*, Helsinki, Finland, 2022, pp. 1-6.

[4] YILMAZ Ü, Güler Ü "On Orbit Demonstration of Pointing Accuracy of Ground Antennas by a Flying GEO Satellite." *Sakarya University Journal of Computer and Information Sciences (Online)*, 6, ss.32 - 36, 2023.

[5] Elorbany K, BAYILMIS C, BALTA S "A Smart Socket Equipped With IoT Technologies for Energy Management of Electrical Appliances." *Sakarya University Journal of Computer and Information Sciences (Online)*, 4, ss.347 - 353, 2021.

[6] ARAT F, Demirci S "Experimental Analysis of Energy Efficient and QoS Aware Objective Functions for RPL Algorithm in IoT Networks." *Sakarya University Journal of Computer and Information Sciences (Online)*, 4, ss.192 - 203, 2021.

[7] M. Di Renzo *et al.*, "Reconfigurable Intelligent Surfaces vs. Relaying: Differences, Similarities, and Performance Comparison," in *IEEE Open J. Commun. Soc.*, vol. 1, pp. 798-807, 2020.

[8] T. L. Jensen and E. De Carvalho, "An Optimal Channel Estimation Scheme for Intelligent Reflecting Surfaces Based on a Minimum Variance Unbiased Estimator," in *Proc. IEEE ICASSP*, Barcelona, Spain, 2020, pp. 5000-5004.

[9] Q. -U. -A. Nadeem, H. Alwazani, A. Kammoun, A. Chaaban, M. Debbah and M. -S. Alouini, "Intelligent Reflecting Surface-Assisted Multi-User MISO Communication: Channel Estimation and Beamforming Design," in *IEEE Open J. Commun. Soc.*, vol. 1, pp. 661-680, 2020.

[10] R. V. Şenyuva, "Channel Estimation for RIS aided MISO System," *SIU*, Istanbul, Turkiye, 2023, pp. 1-4.

[11] Z. Wang, L. Liu and S. Cui, "Channel Estimation for Intelligent Reflecting Surface Assisted Multiuser Communications," in *IEEE WCNC*, Seoul, Korea (South), 2020, pp. 1-6.

[12] G. T. de Araújo, A. L. F. de Almeida and R. Boyer, "Channel Estimation for Intelligent Reflecting Surface Assisted MIMO Systems: A Tensor Modeling Approach," in *IEEE J. Sel. Topics in Signal Process.*, vol. 15, no. 3, pp. 789-802, April 2021.

[13] L. Wei, C. Huang, G. C. Alexandropoulos and C. Yuen, "Parallel Factor Decomposition Channel Estimation in RIS-Assisted Multi-User MISO Communication," in *IEEE SAM*, Hangzhou, China, 2020, pp. 1-5.

[14] L. Wei, C. Huang, G. C. Alexandropoulos, C. Yuen, Z. Zhang and M. Debbah, "Channel Estimation for RIS-Empowered Multi-User MISO Wireless Communications," in *IEEE Trans. Commun.*, vol. 69, no. 6, pp. 4144-4157, June 2021.

[15] C. Beldi, A. Dziri, F. Abdelkefi and H. Shaiek, "PARAFAC Decomposition based Channel Estimation for RIS-aided Multi-User MISO Wireless Communications," in *IWCMC*, Marrakesh, Morocco, 2023, pp. 1537-1542.

[16] K. Ardah, S. Gherekhloo, A. L. F. de Almeida and M. Haardt, "Double-RIS Versus Single-RIS Aided Systems: Tensor-

Based MIMO Channel Estimation and Design Perspectives," in *Proc. IEEE ICASSP*, Singapore, 2022, pp. 5183-5187.
[17] T. G. Kolda and B. W. Bader, "Tensor decompositions and applications," *SIAM Rev.*, vol. 51, no. 3, pp. 455-500, 2009.
[18] P. Comon, X. Luciani, and A.L.F. de Almeida, "Tensor decompositions, alternating least squares and other tales," *J. Chemometrics*, vol. 23, no. 7-8, pp. 393-405, 2009.

Conflict of Interest Notice
The author declare that there is no conflict of interest regarding the publication of this paper.

Ethical Approval and Informed Consent
It is declared that during the preparation process of this study, scientific and ethical principles were followed, and all the studies benefited from are stated in the bibliography.

Availability of data and material
Not applicable

Plagiarism Statement
This article has been scanned by iThenticate ™.